Appl. Chem. Eng., Vol. 33, No. 1, February 2022, 113-118
https://doi.org/10.14478/ace.2021.1108

Article

One-pot Synthesis of Multifunctional Mn_3O_4/mesoporous Silica Core/shell Nanoparticles for Biomedical Applications

Dong Jun Lee, Nohyun Lee* and Ji Eun Lee,†**

School of Chemical and Biological Engineering, Seoul National University, Seoul 08826, Republic of Korea
**School of Advanced Materials Engineering, Kookmin University, Seoul 02707, Republic of Korea*
***School of Chemical Engineering, Chonnam National University, Gwangju 61186, Republic of Korea*
(Received December 23, 2021; Revised January 3, 2022; Accepted January 7, 2022)

Abstract

Multifunctional nanomaterials based on mesoporous silica nanoparticles (MSN) and metal oxide nanocrystals are among the most promising materials for theragnosis because of their ease of modification and high biocompatibility. However, the preparation of multifunctional nanoparticles requires time-consuming multistep processes. Herein, we report a simple one-pot synthesis of multifunctional Mn_3O_4/mesoporous silica core/shell nanoparticles (Mn_3O_4@mSiO_2) involving the temporal separation of core formation and shell growth. This simple procedure greatly reduces the time and effort required to prepare multifunctional nanoparticles. Despite the simplicity of the process, the properties of nanoparticles are not markedly different from those of core/shell nanoparticles synthesized by a previously reported multistep process. The Mn_3O_4@mSiO_2 nanoparticles are biocompatible and have potential for use in optical imaging and magnetic resonance imaging.

Keywords: *One-pot synthesis, Mesoporous silica, MRI contrast agent*

1. Introduction

Nanomaterials have attracted considerable attention for potential applications in various areas because of their unique properties[1]. Among the many nanostructured materials, mesoporous silica nanoparticles (MSN) have been extensively investigated for their potential applications in biomedicine owing to their high biocompatibility, large surface area, large pore volume, uniform and well-defined pore structure, and ease of modification[2]. The functionalization of the pores with stimuli-sensitive ligands enables controlled release of their cargo [3]. Furthermore, advanced multifunctional applications become possible when MSN are combined with other nanoparticles[4]. In particular, metal oxide nanoparticles, which have been employed as novel magnetic resonance imaging (MRI) contrast agents, endow MSN with diagnostic capability, resulting in multifunctional nanoparticles[5]. These multifunctional nanoparticles will play an important role in enabling simultaneous diagnosis and therapy (theragnosis)[6]. However, most current methods of synthesizing multifunctional mesoporous-silica-based nanoparticles are time-consuming and cumbersome. These multifunctional nanoparticles have usually been synthesized by the formation of a silica shell around an individual nanoparticle[5] or by the decoration of the silica surface with multiple nanoparticles[7]. These methods, however, require complicated and laborious synthesis, separation, and washing processes. For instance, to synthesize multifunctional nanoparticles composed of a metal oxide core and a mesoporous silica shell, the core materials are initially prepared by a thermal decomposition reaction, followed by isolation and multiple washing steps[8]. Subsequently, additional phase transfer using cetyltrimethlyammonium bromide (CTAB) is needed to disperse the nanoparticles in an aqueous phase. Finally, mesoporous silica shells are generated by hydrolysis/condensation of silica precursors such as tetraethoxysilane (TEOS), which also requires isolation and multiple washing steps[5].

Herein, we present a one-pot synthetic method to fabricate multifunctional Mn_3O_4/mesoporous silica core/shell nanoparticles (designated as Mn_3O_4@mSiO_2 nanoparticles). One of the simplest ways to synthesize metal oxide nanoparticles, including manganese oxide nanoparticles, is precipitation, where metal salts are reacted under basic conditions[9]. Interestingly, basic conditions have also been used in the sol–gel reaction of silane precursors to form silica nanostructures[10]. Inspired by the feasibility of employing basic conditions in both synthetic procedures, we developed a one-pot synthetic process for Mn_3O_4@mSiO_2 nanoparticles. This method does not require laborious synthesis, separation, or multiple washing steps for the core Mn_3O_4 nanoparticles; moreover, it does not involve any additional phase-transfer-mediated dispersion step. The synthesized Mn_3O_4@mSiO_2 nanoparticles retain the original characteristics of each component and exhibit multifunctionality similar to that of core/shell nanoparticles fabricated by a previously reported multistep process[5]. Similar to conventional MSN, the overall size, optical properties, and pore size of the Mn_3O_4@mSiO_2 nanoparticles can be easily controlled. The paramagnetic Mn_3O_4 core enhances the longitudinal relaxation of water

† Corresponding Author: Chonnam National University
School of Chemical Engineering, Gwangju 61186, Republic of Korea
Tel: +82-62-530-1843 e-mail: jelee@jnu.ac.kr

pISSN: 1225-0112 eISSN: 2288-4505

protons, exhibiting r_1 relaxivity comparable to that of solid manganese oxide nanoparticles, which have been employed as a novel T_1 MRI contrast agent to avoid the toxic side effects of gadolinium complexes, such as nephrogenic system fibrosis[11].

2. Materials and method

2.1. Synthesis of Mn_3O_4@$mSiO_2$ nanoparticles

Mn_3O_4@$mSiO_2$ nanoparticles were synthesized by a slight modification of a previously reported method[12]. Typically, CTAB (Acros, 99+%) (50 mg) and $MnCl_2 \cdot 4H_2O$ (Sigma-Aldrich, >98%) (24 mg) were mixed in 50 mL of deionized water at room temperature. The mixture was heated to 70 °C at 2 °C/min under vigorous magnetic stirring. During heating, a NaOH solution (350 μL, 2 M) was added at 50 °C to induce the formation of Mn_3O_4 nanoparticles. When the temperature of the mixture reached 70 °C, 800 μL of TEOS (Acros, 98%) and 3 mL of ethyl acetate (Samchun, 99.5%) were added, and the mixture was aged for 6 h. The synthesized nanoparticles were collected by centrifugation and washed several times with water and ethanol. To remove the pore-generating template CTAB, the product was dissolved in 50 mL of ethanol containing 0.1 g of NH_4NO_3 (Sigma-Aldrich, > 98%) and stirred at 60 °C for 1 h. For synthesis of fluorescence dye-doped nanoparticles (Mn_3O_4@$mSiO_2$-FITC or Mn_3O_4@$mSiO_2$-RITC), 3-aminopropyltriethoxysilane (APTES, Sigma, 98%) was conjugated with Rhodamine B isothiocyanate (RITC, Aldrich) (5 mg) or fluorescein isothiocyanate (FITC, Aldrich) (4 mg) (molar ratio of dye : APS = 1:10) in 1 mL of ethanol overnight in the dark. In the same process as the above synthesis method for Mn_3O_4@$mSiO_2$ nanoparticles, dye-conjugated APTES in an amount corresponding to 10% of TEOS is added together with TEOS.

2.2. PEGylation of Mn_3O_4@$mSiO_2$ nanoparticles

The surfaces of the nanoparticles were PEGylated by covalent bonding between the primary amine-functionalized nanoparticles and succinimide-terminated polyethylene glycol (PEG). In detail, template-free Mn_3O_4@$mSiO_2$ nanoparticles were dissolved in 20 mL of anhydrous ethanol, and APTES was added to the solution. After the mixture was refluxed for 3 h, the amine-functionalized Mn_3O_4@$mSiO_2$ nanoparticles were centrifuged and washed with ethanol. For PEGylation, 50 mg of mPEG-SG (succinimidyl-glutarate-terminated PEG, 5000 Da, Sunbio) was added to the nanoparticles, and the mixture was aged for 12 h. The final product was collected by centrifugation and washed.

2.3. Characterization of Mn_3O_4@$mSiO_2$ nanoparticles

The shape and structure of the nanoparticles were characterized using transmission electron microscopy (TEM, JEM-2010, JEOL) at 200 kV. For TEM analysis, microfilms were prepared by placing a drop of the nanoparticle dispersion on a 200-mesh copper TEM grid and subsequent drying at room temperature for 2 h. The crystal structure of the nanoparticles was evaluated via X-ray diffraction (XRD, D/Max-3C diffractometer, Rigaku) analysis using Cu Kα radiation (λ = 0.15418 nm). Nitrogen adsorption/desorption isotherms were obtained using a 3FLEX surface characterization analyzer (Micromeritics). The concentration of manganese ions was measured by inductively coupled plasma atomic emission spectroscopy (ICPS-7500 spectrometer, Shimadzu).

2.4. Measurement of MR relaxation properties

The MR relaxivities of the Mn_3O_4@$mSiO_2$ nanoparticles were measured using a clinical 3 T MR scanner (TrioTrim, Siemens) with a head coil. The inversion recovery fast spin-echo sequence was used to measure T_1. The measurement parameters were as follows: TR = 4000 ms, TE = 14 ms, and TI = 25−3500 ms.

2.5. In vitro cytotoxicity against U87MG cells

Cells were grown in Dulbecco's modified Eagle's medium (Gibco) supplemented with 10% (v/v) fetal bovine serum (Gibco) and penicillin/streptomycin (100 U/mL and 100 μg/mL, respectively, Gibco) at 37 °C in humidified 5% CO_2 atmosphere. For *in vitro* cytotoxicity assay, cells in a logarithmic growth phase were detached and plated (0.2 mL per well) on 96-well flat-bottom microplates at a density of 10,000 cells per well and left for 1−2 days at 37 °C to resume exponential growth. After the cells were washed with PBS, 0.1 mL of a culture medium with a given concentration of nanoparticles was added to the wells in quintuplicate. For the control wells, the same volume of culture medium was used in each experiment. Following 24 h of continuous exposure to the nanoparticles, the cells were incubated in media with 0.1 mg/mL of 3-(4,5-dimethylthialzol-2-yl)-2,5-diphenyltetrazolium bromide (MTT, Sigma) for 1 h. Next, the MTT solution was removed, and the precipitated violet crystals were dissolved in 0.2 mL of dimethyl sulfoxide. The absorbance was measured at 560 nm using a Victor X4 Multilabel Plate Reader (PerkinElmer).

3. Results and discussion

The procedure for the fabrication of Mn_3O_4@$mSiO_2$ nanoparticles is illustrated in Figure 1. At the beginning of the synthesis, an aqueous CTAB solution containing manganese(II) chloride was heated to 70 °C. When the temperature reached 50 °C, sodium hydroxide solution was added to the solution under vigorous stirring, which immediately induced the formation of Mn_3O_4 cores approximately 10 nm in size[13]. It is noteworthy that CTAB acts not only as a pore-generating template, but also as a stabilizing surfactant for the Mn_3O_4 nanoparticles. The Mn_3O_4 nanoparticles exhibited high dispersibility owing to stabilization by CTAB but were severely aggregated in the absence of CTAB. Subsequently, without a separation step, mesoporous silica shells were generated by the direct addition of TEOS to the basic solution containing Mn_3O_4-CTAB. The TEM images in Figure 2 reveal the core/shell structure of the obtained Mn_3O_4@$mSiO_2$ nanoparticles. The nanoparticles were essentially spherical in shape, with slight variation depending on the shape of the aggregates in the Mn_3O_4 cores [Figure 2(a)]. The high-resolution TEM image clearly reveals the wormhole-like mesoporous structures of the silica shell derived from the CTAB template[Figure 2(b)]. The crystal structure of the Mn_3O_4@$mSiO_2$ nanoparticles was determined by XRD, as shown in

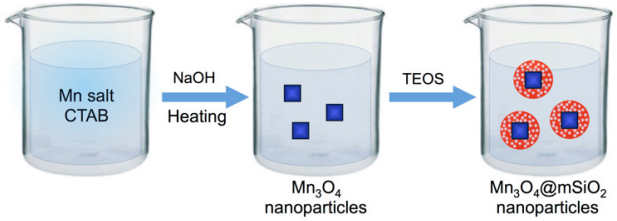

Figure 1. Schematic of one-pot synthetic procedure for Mn_3O_4 core/mesoporous silica shell (Mn_3O_4@$mSiO_2$) nanoparticles.

Figure 2(c). The broad peak around 2θ = 22° was attributed to the characteristic diffraction of amorphous silica (JCPDS No. 29-0085). The other XRD peaks were assigned to tetragonal Mn_3O_4 (JCPDS No. 18-0803). No diffraction peaks corresponding to cubic MnO were observed.

In a one-pot synthesis system, all the reactions must occur in the same reaction vessel; thus, temporal separation between the formation of the Mn_3O_4 core and the growth of the mesoporous silica shell plays a critical role in obtaining discrete core/shell structures. This separation can be achieved by the sequential addition of reagents, i.e., sodium hydroxide followed by TEOS, which provides a time interval between core and shell formation. When TEOS and other reagents were added at room temperature at the beginning of the synthesis, sheet-like Mn_3O_4 cores were formed, and the resulting core/shell nanoparticles were severely aggregated. In this case, small silica nanoparticles were also generated, as shown in Figure 3(a). The reason is that the manganese salt affected the condensation of TEOS, and vice versa. Under the standard reaction conditions in the absence of the manganese salt, discrete MSN without a core were obtained[Figure 3(b)]. From these results, we conclude that the temporal separation of core formation and shell growth is critical for the synthesis.

The thickness of the mesoporous silica shell can easily be tuned from 10 to 40 nm by varying the amount of TEOS added during shell formation. With increasing TEOS concentration, the thickness of the shell and the overall size of the resulting nanoparticles increased [Figure 4(a)-(c)]. Moreover, the thickness of the silica shell was affected by the concentration of manganese(II) chloride. When the amount of manganese salt was tripled, the thickness of the silica shell decreased from 40 to 25 nm, whereas the shape and size of the Mn_3O_4 core remained the same[Figures 4(d) and (e)]. This result indicates that the concentration of manganese(II) chloride affects the number of Mn_3O_4 cores rather than their size. Thus, it can be concluded that the silica shell thickness is determined mainly by the ratio of the silica source (TEOS) and manganese(II) chloride.

To endow the Mn_3O_4@$mSiO_2$ nanoparticles with fluorescence imaging capability, fluorescent dyes, such as FITC and RITC, were incorporated covalently into the silica shells by the co-condensation of dye-conjugated APTES with TEOS. TEM images of the dye-doped nanoparticles indicated that the incorporation of dyes did not affect the size and shape of the obtained nanoparticles[Figures 5(a) and (b)]. Photoluminescence (PL) measurements of the dye-doped nanoparticles (Mn_3O_4@$mSiO_2$-FITC and Mn_3O_4@$mSiO_2$-RITC) revealed the characteristic emissions of fluorescein and rhodamine B at 520 nm (λ_{ex} = 470 nm) and 560 nm (λ_{ex} = 520 nm), respectively[Figure 5(c)].

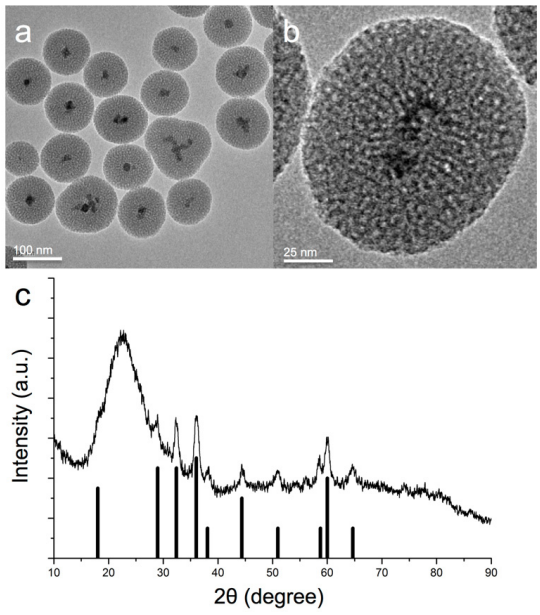

Figure 2. (a) TEM image and (b) high-resolution TEM image of Mn_3O_4@$mSiO_2$ nanoparticles. (c) XRD pattern of Mn_3O_4@$mSiO_2$ nanoparticles. Bottom line shows the pattern of tetragonal Mn_3O_4 (JCPDS No. 18-0803).

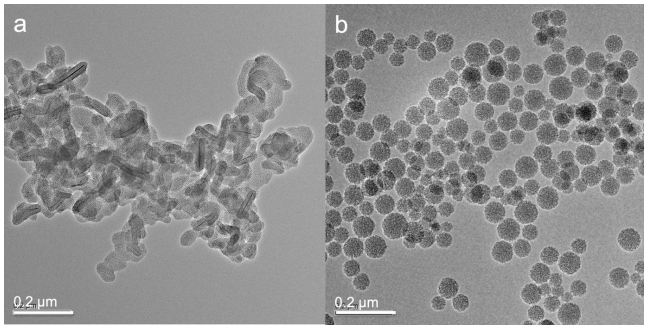

Figure 3. (a) TEM image of Mn_3O_4@$mSiO_2$ nanoparticles synthesized with the initial addition of TEOS at room temperature. (b) TEM image of mesoporous silica nanoparticles obtained under the same conditions, except that no manganese salt was added.

To utilize the large pore volume in mesoporous structures, pore-generating templates such as CTAB should be removed from the as-synthesized nanoparticles. The organic template is typically removed by acid treatment[5] or calcination[14]. However, in this study, acid treatment was ruled out because the Mn_3O_4 core is likely to dissolve at low pH[15]. In addition, calcination would burn away organic dyes as well as templates. Thus, in our experiments, CTAB was successfully removed via ion exchange with NH_4^+ cations[16]. The mild conditions in the ion exchange process, i.e., the use of an ammonium nitrate solution, did not affect the Mn_3O_4 core or the organic fluorescent dyes. N_2 adsorption/desorption measurement of the Mn_3O_4@$mSiO_2$ nanoparticles showed a typical type-IV isotherm with type-H1 hysteresis, demonstrating the successful removal of the CTAB template by treat-

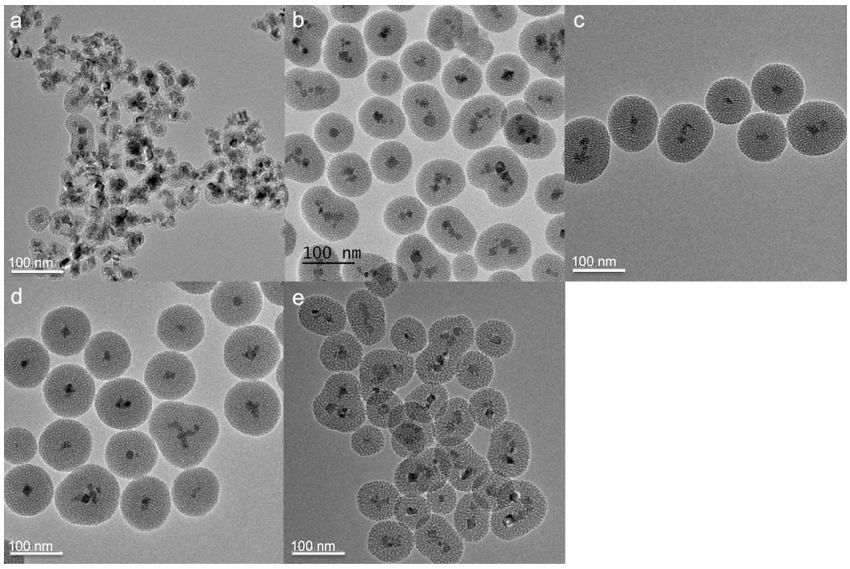

Figure 4. (a-c) TEM images of Mn_3O_4@$mSiO_2$ nanoparticles with mesoporous silica shell thicknesses of (a) 10 nm, (b) 30 nm, and (c) 40 nm, synthesized using 350 μL, 500 μL, and 800 μL of TEOS, respectively. (d-e) TEM images of Mn_3O_4@$mSiO_2$ nanoparticles with mesoporous silica shell thicknesses of (a) 40 nm and (b) 25 nm, synthesized using 24 and 72 mg of manganese salt, respectively.

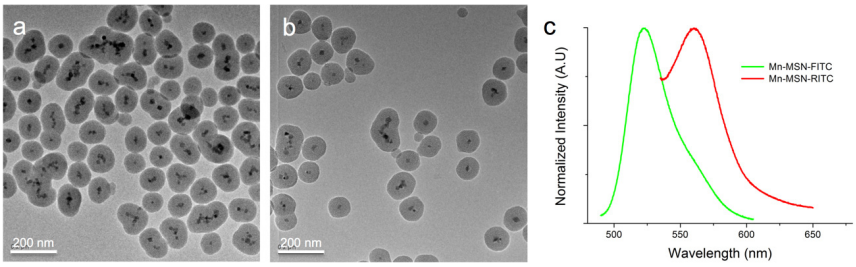

Figure 5. TEM images of (a) Mn_3O_4@$mSiO_2$-FITC and (b) Mn_3O_4@$mSiO_2$-RITC. (c) PL spectra of Mn_3O_4@$mSiO_2$-FITC (green) and Mn_3O_4@$mSiO_2$-RITC (red).

ment with NH_4^+ cations[Figures 6(a) and (b)]. The Brunauer–Emmett–Teller surface area was found to be 582.88 m^2 g^{-1}. The pore size distribution calculated from the desorption branch according to the Barrett–Joyner–Halenda model showed a narrow distribution with an average pore size of 2.3 nm. The pore size of the mesoporous silica shell can be enlarged using pore-expanding agents[17]. When 1,3,5-trimethylbenzene (TMB) was added, the surface area and pore size increased to 617.93 m^2 g^{-1} and 3.92 nm, respectively[Figures 6(c) and (d)].

The cytotoxicity of the Mn_3O_4@$mSiO_2$ nanoparticles was assessed using U87-MG human glioma cell lines incubated with various concentrations of nanoparticles for 24 h and then subjected to MTT assay. Before the *in vitro* test, the Mn_3O_4@$mSiO_2$ nanoparticles were PEGylated to enhance their biocompatibility. The PEGylated nanoparticles exhibited no appreciable toxicity when the Mn concentration was less than 34 μM[Figure 7(a)] [11]. When the cells were incubated with RITC-labeled Mn_3O_4@$mSiO_2$ nanoparticles for 4 h, the red fluorescence of RITC was clearly visible in the cytoplasm, indicating efficient cellular uptake[Figures 7(b)–(d)].

The MR contrast effect of the Mn_3O_4@$mSiO_2$ nanoparticles was investigated using a clinical 3 T MR scanner. Clear signal enhancement was observed in a T_1-weighted MR image[Figure 7(e)]. The measured

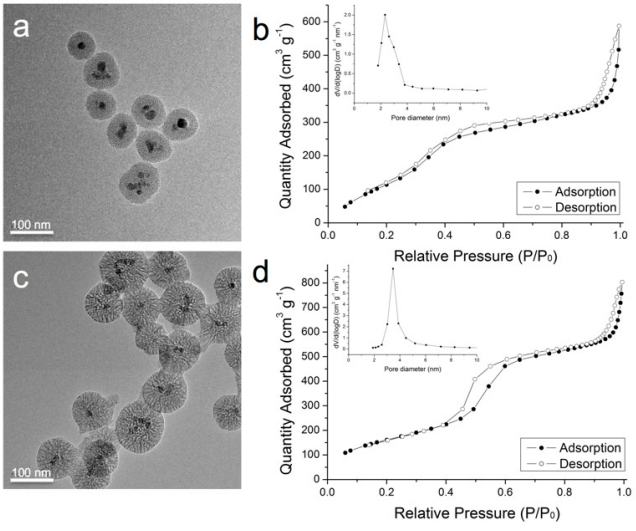

Figure 6. (a) TEM image of Mn_3O_4@$mSiO_2$ nanoparticles after removal of CTAB and (b) their N_2 adsorption/desorption isotherms (inset: pore size distribution from adsorption branch). (c) TEM image of Mn_3O_4@$mSiO_2$ nanoparticles with larger pores derived from pore-expanding agent (TMB) and (d) their N_2 isotherms.

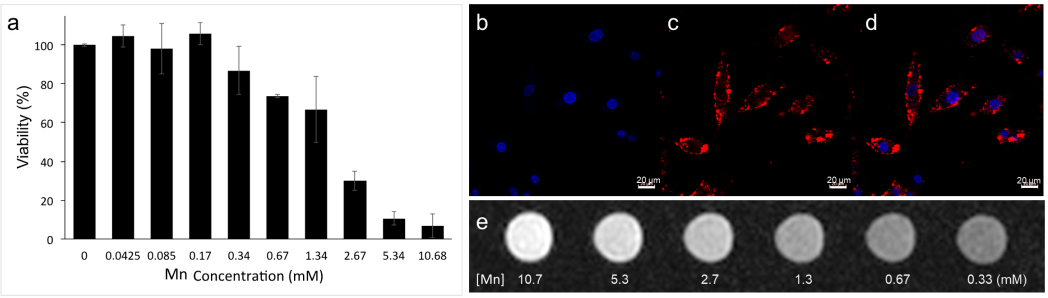

Figure 7. (a) *In vitro* cytotoxicity of PEGylated Mn_3O_4@$mSiO_2$ nanoparticles against U87-MG glioma cell lines after 24 h of incubation. (b–d) Confocal laser scanning microscope images of U87-MG cells incubated with PEGylated Mn_3O_4@$mSiO_2$-RITC. (b) Nuclei stained with blue 4′-6-diamidino-2-phenylindole. (c) Red fluorescence representing internalized nanoparticles. (d) Merged version of images in (b) and (c). (e) T_1-weighted MR image of Mn_3O_4@$mSiO_2$ nanoparticles.

r_1 and r_2 values of the nanoparticles were 0.12 and 1.2 $mM^{-1}s^{-1}$, respectively, which are comparable to the previously reported relaxivities of solid MnO nanoparticles[11]. Given that the MR relaxivity of MnO nanoparticles coated with a dense silica shell is significantly reduced, the mesoporous shell does not seem to affect the longitudinal relaxation process, because it allows water diffusion through the mesopores[15]. These results indicate that the Mn_3O_4@$mSiO_2$ nanoparticles have excellent potential for use as dual optical and MR imaging agents.

4. Conclusions

A one-pot method for the synthesis of a discrete Mn_3O_4/mesoporous silica core/shell nanostructure was developed using the temporal separation of core formation and shell growth. The simple procedure outlined here reduces the time and effort required to prepare multifunctional nanoparticles. Despite the simplicity of the process, the multifunctional properties of Mn_3O_4@$mSiO_2$ are not significantly different from those of core/shell nanoparticles synthesized by established multistep processes. Because of the MRI contrast effect of the Mn_3O_4 core and the optical imaging and drug delivery capability of the mesoporous silica shell, the Mn_3O_4@$mSiO_2$ nanoparticles can be used as multifunctional agents. Further modification of the mesoporous silica shell through well-developed silica chemistry using various organosilane reagents can be applied using our one-pot synthetic process to expand the functionality and application areas of the nanoparticles. Because the co-precipitation of metal salts in alkaline solution is a conventional method for the synthesis of a wide range of nanoparticles, this study can be expanded to include other transition metals such as iron and gadolinium.

Acknowledgements

This work was supported by the National Research Foundation of Korea (NRF) grant funded by the Korea government (MSIT) (No. 2021R1A2C1011317) and Chonnam National University (Grant number : 2021-2505).

References

1. 1. Q. He, S. Guo, Z. Qian, and X. Chen, Development of individualized anti-metastasis strategies by engineering nanomedicines, *Chem. Soc. Rev.*, **44**, 6258-6286 (2015).
2. B. G. Cha and J. Kim, Functional mesoporous silica nanoparticles for bio-imaging applications, *Wiley Interdiscip. Rev. Nanomed. Nanobiotechnol.*, **11**, e1515 (2019).
3. B. Yang, Y. Chen and J. Shi, Exogenous/endogenous-triggered mesoporous silica cancer nanomedicine, *Adv. Healthc. Mater.*, **7**, 1800268 (2018).
4. E. Rastegari, Y.-J. Hsiao, W.-Y. Lai, Y.-H. Lai, T.-C. Yang, S.-J. Chen, P.-I Huang, S.-H. Chiou, C.-Y. Mou and Y. Chien, An update on mesoporous silica nanoparticle applications in nanomedicine, *Pharmaceutics*, **13**, 1067 (2021).
5. J. Kim, H. S. Kim, N. Lee, T. Kim, H. Kim, T. Yu, I. C. Song, W. K. Moon, and T. Hyeon, Multifunctional uniform nanoparticles composed of a magnetite nanocrystal core and a mesoporous silica shell for magnetic resonance and fluorescence imaging and for drug delivery, *Angew. Chem. Int. Ed.*, **47**, 8438-8141 (2008).
6. D. E. Lee, H. Koo, I.-C. Sun, H. J. Ryu, K. Kim, and I. C. Kwon, Multifunctional nanoparticles for multimodal imaging and theragnosis, *Chem. Soc. Rev.*, **41**, 2656-2672 (2012).
7. J. E. Lee, N. Lee, H. Kim, J. Kim, S. H. Choi, J. H. Kim, T. Kim, I. C. Song, S. P. Park, W. K. Moon, and T. Hyeon, Uniform mesoporous dye-doped silica nanoparticles decorated with multiple magnetite nanocrystals for simultaneous enhanced magnetic resonance imaging, fluorescence imaging, and drug delivery, *J. Am. Chem. Soc.*, **132**, 552-557 (2010).
8. J. Park, K. An, Y. Hwang, J. Park, H. Noh, J. Kim, J. Park, N. Hwang, and T. Hyeon, Ultra-large-scale syntheses of monodisperse nanocrystals, *Nat. Mater.*, **3**, 891-895 (2004).
9. M. Worden, M. A. Bruckman, M. H. Kim, N. F. Steinmetz, J. M. Kikkawa, C. LaSpina, and T. Hegmann, Aqueous synthesis of polyhedral “brick-like” iron oxide nanoparticles for hyperthermia and T_2 MRI contrast enhancement, *J. Mater. Chem. B*, **3**, 6877-6884 (2015).
10. A. Guerrero-Martinez, J. Perez-Juste, and L. M. Liz-Marzan, Recent progress on silica coating of nanoparticles and related nanomaterials, *Adv. Mater.*, **22**, 1182-1195 (2010).
11. H. B. Na, J. H. Lee, K. An, Y. I. Park, M. Park, I. S. Lee, D.-H. Nam, S. T. Kim, S,-H. Kim, S.-W. Kim, K.-H. Lim, K.-S. Kim,

S.-O. Kim, and T. Hyeon, Development of a T1 contrast agent for magnetic resonance imaging using MnO nanoparticles, *Angew. Chem. Int. Ed.*, **46**, 5397-5401 (2007).
12. P. S. Mueller, C. P. Parker, and S. C. Larsen, One-pot synthesis of iron oxide mesoporous silica core/shell nanocomposites, *Micropor. Mesopor. Mat.*, **204**, 173-179(2015).
13. X. Li, L. Zhou, J. Gao, H. Miao, H. Zhang, and J. Xu, Synthesis of Mn_3O_4 nanoparticles and their catalytic applications in hydrocarbon oxidation, *Powder Technol.*, **190**, 324-326 (2009).
14. K.-C. Kao, C.-H. Lin, T.-Y. Chen, Y.-H. Liu, and C.-Y. Mou, A general method for growing large area mesoporous silica thin films on flat substrates with perpendicular nanochannels, *J. Am. Chem. Soc.*, **137**, 3779-3782 (2015).
15. T. Kim, E. Momin, J. Choi, K. Yuan, H. Zaidi, J. Kim, M. Park, N. Lee, M. T. McMahon, A. Quinones-Hinojosa, J. W. M. Bulte, T. Hyeon, and A. A. Gilad, Mesoporous silica-coated hollow manganese oxide nanoparticles as positive T_1 contrast agents for labeling and MRI tracking of adipose-derived mesenchymal stem cells, *J. Am. Chem. Soc.*, **133**, 2955-2961 (2011).
16. N. Lang, and A. Tuel, A fast and efficient ion-exchange procedure to remove surfactant molecules from MCM-41 materials, *Chem. Mater.*, **16**, 1961-1966 (2004).
17. J. Fan, C. Yu, T. Gao, J. Lei, B. Tian, L. Wang, Q. Luo, B. Tu, W. Zhou, and D. Zhao, Cubic mesoporous silica with large controllable entrance sizes and advanced adsorption properties, *Angew. Chem. Int. Ed.*, **42**, 3146-3150 (2003).

Authors

Dong Jun Lee; Ph.D., Researcher, School of Chemical and Biological Engineering, Seoul National University, Seoul 08826, Korea; ldj1807@snu.ac.kr

Nohyun Lee; Ph.D., Professor, School of Advanced Materials Engineering, Kookmin University, Seoul 02707, Korea; nohyunlee@kookmin.ac.kr

Ji Eun Lee; Ph.D., Professor, School of Chemical Engineering, Chonnam National University, Gwangju 61186, Korea; jelee@jnu.ac.kr